J Mater Sci: Mater Electron (2016) 27:843–851
DOI 10.1007/s10854-015-3825-2

Modification of TiO_2 nanoparticles by HZSM-5 for the enhancement in photodegradation of Acid Green 25

M. B. Suwarnkar[1] · A. N. Kadam[1] · G. V. Khade[1] · N. L. Gavade[1] · K. M. Garadkar[1]

Received: 15 May 2015 / Accepted: 2 October 2015 / Published online: 7 October 2015

Abstract A great approach for the preparation of TiO_2 supported on HZSM-5 photocatalyst was employed by an energy efficient microwave assisted technique. Titanium tetraisopropoxide (TTIP) was used as a titanium precursor and medium pore size HZSM-5 with high thermal and chemical resistance used as a support. The amount of TTIP was varied in order to obtain different TiO_2 loading of 20, 30 and 40 wt% on HZSM-5. The obtained nanomaterials were studied by a set of complementary characterization techniques including X-ray diffraction, transmission electron microscopy, scanning electron microscopy, energy dispersive spectroscopy, Fourier transform-infrared spectroscopy, surface area measurement (BET) and diffuse reflectance spectroscopy. The present research is mainly focused on the enhancement of surface area of TiO_2 nanoparticles by using HZSM-5 as a support. The obtained nanomaterials were tested for the degradation of Acid Green 25 under UV light (365 nm). A maximum 96 % photodegradation of dye was achieved by utilizing most efficient TiO_2(30 %)/HZSM-5 at 0.1 g/dm^3 catalyst within 60 min under UV light.

1 Introduction

In the past decade, nanostructure materials have been received considerable attention due to their unique physicochemical properties and large number of unique applications [1–3]. In particular semiconductor photocatalysis encompasses a number of diverse and related disciplines in Science and Engineering. It has been applied for mitigating environmental pollutants, wastewater treatment, generating solar cells and inhibition of bacteria, viruses etc. [4]. The most widely used semiconductor photocatalyst is TiO_2 which become a "gold standard" in photocatalysis. Its popularity stems due to easy and inexpensive method of preparation, highly stable in aqueous medium, non-toxic and capable to degrade several classes of pollutants [5–7].

Apart from this, nanoparticles of titania has certain limitations such as tendency of aggregation in suspension that rapidly lose their effective surface area, being a non-porous in nature, it exhibits low adsorption ability and low quantum degradation efficiency for pollutants [8]. The photocatalytic activity of TiO_2 is greatly influenced by crystal structure, particle size, porosity and surface area. Enhancement in the surface area of TiO_2 is the most noticeable mean to improve the efficiency of photocatalytic oxidation reactions [9–12]. Extensive efforts on research is underway the world over for the development of suitable high surface area photocatalyst. Therefore several attempts were made to support fine particles of TiO_2 on porous materials of large surface area using adsorbents like silica, alumina, clay, zeolite and activated carbon. Among these materials, great attention has been focused on zeolite due to its unique properties like uniform pores and channel sizes (3–8 Å). These studies have been built-in an effort to enhance the adsorption of reactant on the catalyst surface to improve the catalytic efficiency of photocatalysis [13, 14].

HZSM-5 zeolite is crystalline inorganic microporous, aluminosilicate and material, consisting of a three-dimensional (3D) SiO_4 and AlO_4 tetrahedral associated with interconnecting oxygen ions having an inverted mordenite framework (MFI) structure [15]. HZSM-5 with three

✉ K. M. Garadkar
kmg_chem@unishivaji.ac.in

[1] Nanomaterials Research Laboratory, Department of Chemistry, Shivaji University, Kolhapur 416004, India

dimensional pore system consisting of sinusoidal (5.3 × 5.6 Å) and straight (5.2 × 5.7 Å) channel was shown to be more effective in promoting the catalytic reaction. Whenever Al^{3+} replaces Si^{4+}, an additional proton (H^+) will be required to maintain electrical neutrality. These additional protons will provide a high degree of acidity to HZSM-5 [16]. It holds regular periodic structure with channels and cages which endow the catalyst unique structure, strong adsorption capability, large surface area and chemically stable in nature [17]. Therefore in this study an effort is made to support TiO_2 on HZSM-5 so as to enhance the photocatalytic activity for a wide range of industrial processes. Therefore, HZSM-5 type materials are the catalysts of choice for a wide range of industrial processes. The HZSM-5 type in particular is used in a number of catalytic processes such as conversion of oxygenates (methanol and dimethyl ether) into olefins, fluid catalytic cracking (FCC), alkylation of aromatics, ethyl-benzene production, and xylene isomerization.

Reddy et al. [18] reported on the study of photocatalytic degradation of phenol by using TiO_2, Al-MCM-41 and different wt% loading of TiO_2 on Al-MCM-41. The photocatalytic activity of the supported TiO_2 systems was found to be high in comparison with pristine TiO_2. In this report TiO_2 (10 %)/Al-MCM-41 shows complete mineralization of phenol within 2 h (99.9 %) where as 18 and 90 % by Al-MCM-41 and pristine TiO_2 respectively. Young et al. [19] reported on the degradation of Chlorazole Black E over zeolite supported titanium based catalyst. It was found that, the COD of dye solution was decreased at pH 6 (45 %) and at pH 11 (30 %) whereas it is increased at pH 2 (25 %). The decrease in COD with zeolite supported catalyst was observed as compared to pristine TiO_2. From this research work we observed that, supported TiO_2 found to be more efficient as compared to pristine TiO_2. Therefore, we are paying more attention towards the enhancement of photocatalytic activity of TiO_2 supported on HZSM-5.

Synthetic dyes have a strong resistance to fading while simultaneously providing an array of bright colors in the modern textile products. Guidelines and regulations for proper disposal and treatment have become mandatory in order to protect the environment and human health. Because of this fact, many researchers have paid more attention to develop effective methods to remediate synthetic dyes. The most prominent degradation process can be referred as advanced oxidation processes (AOP). AOP's are associated with the aqueous phase production of the hydroxyl radical that result in the destruction of the target pollutant.

The AG 25 is employed as a model pollutant and it is stable (not readily decomposed) in water at 20 °C up to 7 days. As a result, some aquatic organisms and plants might be compromised. Moreover, this dye also brought about a slight or spotty discoloration in the orbital tissue of some animals at 10 % aqueous solution, very mild irritation at 15 % aqueous solution and dermal irritation at 50 % aqueous solution in 1 % carboxymethyl cellulose (CMC), hence degradation of AG-25 is an important task [20]. Many researchers have reported on the photocatalytic activity of TiO_2/HZSM-5 as a catalyst for the degradation of various dyes.

In the present study, we have accounted for the synthesis of TiO_2 supported on HZSM-5 by an energy efficient microwave method. The photocatalytic studies were evaluated by using AG 25 as a model pollutant. To get the maximum photodegradation of dye, a series of experiments were carried out such as effect of loading of TiO_2 on HZSM-5, calcination temperature and catalyst loading, etc. This will be the first investigation to report on the HZSM-5 supported TiO_2 photocatalyst for the degradation of AG 25.

2 Experimental

2.1 Materials

Titanium tetra-isopropoxide (TTIP, 99 %), Cetyl Trimethyl Ammonium Bromide (CTAB, 99 %) were purchased from Spectrochem Pvt. Ltd., (India). Absolute ethanol (99.9 %) was purchased from SD. fine chemicals. sodium dodecyl sulfate (SDS, extrapure) was purchased from Thomas Baker Pvt. Ltd., Mumbai and 25 % Ammonia was purchased from Loba Chemie Pvt. Ltd., (India). All analytical grade chemicals were used as received for the preparation of solutions. All solutions were prepared in Millipore water obtained from Millipore water system (Bangalore, India).

2.2 Photocatalyst preparation

TTIP was used as a source of titanium. The supported catalyst was prepared by taking controlled addition of TTIP (0.1 M) in ethanol with constant stirring to get a clear solution. An adequate amount of surfactant (1 % CTAB + 1 % SDS) was added with constant stirring. The HZSM-5 was prepared by a known method [21] which added in solution and kept for stirring. An aqueous solution of ammonia was added dropwise with stirring condition at room temperature until solution reached up to pH = 8. The amount of TTIP was varied to generate insitu TiO_2 loading about 20, 30 and 40 wt% in the final solid photocatalyst, and they were assigned as TiO_2 (20 %)/HZSM-5, TiO_2 (30 %)/HZSM-5 and TiO_2(40 %)/HZSM-5, respectively. After complete precipitation, the precipitate was washed with water and acetone for several times to remove excess surfactant and other impurity. The washed precipitate was

kept under microwave irradiation for 20 min in microwave oven (Input 900 W, 250 MHz, LG Make) with on–off cycle (20 s on-40 s off). The dried powder was grounded by using agate mortar and pestle. The catalyst TiO_2 (30 %)/HZSM-5 was calcined at various temperatures from 300 to 600 °C. The phase purity and degree of crystallinity of pristine TiO_2 and HZSM-5 supported TiO_2 were monitored by X-ray diffraction (XRD).

2.3 Characterization method

In order to investigate the size of crystals and phase purity of pristine and supported TiO_2, the powder was subjected to XRD using an X-ray diffractometer (Model X-Pert PRO-1712) with CuKα radiation (λ = 1.5406 Å) as an X-ray source. The particle size of the material was obtained by using transmission electron microscopy with model TEM (JEOL 3010). The morphological features and elemental composition of pristine and supported TiO_2 obtained by energy dispersive spectroscopy attached to a SEM. FT-IR spectrum was recorded on the Spectrum-one (Perkin Elmer) in the range of 4000–400 cm^{-1} using KBr pellet. The surface area of the sample was determined by using BET (Micromeritics-2720) under 30 % nitrogen in a helium environment at 77 K. The diffuse reflectance spectrum (DRS) of powder was recorded at room temperature using a Spectrophotometer (Varian Cary-5000).

2.4 Photocatalytic activity

The photocatalytic activity of pristine and supported TiO_2 was tested for the degradation of AG 25 as a model pollutant under UV light. To investigate the highest photocatalytic activity of supported TiO_2, the amount of catalyst was varied from 0.05 to 0.125 g/dm^3. The quartz photoreactor was kept in a steel container along with magnetic stirrer. High pressure mercury lamp (Philips HPL-N, 250 W) was used as a light source which has Lumens of 12750. The outer cover of the bulb was broken and just inside filament was used as a source of light. The lamp was kept 5 cm above the dye solution. In the known experiment the photocatalyst was added in photoreactor containing 100 mL of AG 25 (25 ppm). Before irradiation, dye solution was stirred for 30 min in dark to ensure adsorption–desorption equilibrium. All photodegradation experiments performed at ambient temperature with similar experimental condition, then at a particular time interval aliquots withdrawn and centrifuged to remove suspended particles of photocatalyst. Then absorbance of the clear solution was recorded by using UV–Vis–NIR spectrophotometer (Shimadzu, Model-UV-3600) to examine the concentration of dye.

3 Results and discussion

3.1 Characterization of TiO_2/HZSM-5 catalyst

3.1.1 XRD of TiO_2/HZSM-5

Figure 1 shows the XRD patterns of HZSM-5, TiO_2, and different wt% of TiO_2 supported on HZSM-5. From the XRD pattern for the HZSM-5, the peaks observed at 2 theta values 7.95, 8.83, 13.95, 14.83, 15.93, 20.88, 23.18, 23.99, 30.09 and 45.59 corresponds to [011], [200], [102], [301], [202], [113], [501], [303], [053] and [0 10 0] respectively. The crystal planes confirms the highly crystalline phase of HZSM-5 in inverted mordenite framework (MFI) structure with orthorhombic form which is similar to those of the standard reference for a highly pure HZSM-5 [22]. The supported sample indicates the characteristic peaks of both TiO_2 and HZSM-5, which shows that the crystal structure of HZSM-5 is protected during the synthesis of nano TiO_2. The diffraction pattern of supported photocatalyst show peaks at 25.11°, 37.87°, 47.92° and 55.02° which are assigned to the reflections from [101], [004], [200] and [211] planes of anatase phase respectively [23] this attributed to reflections of anatase TiO_2 which is compared with $JCPD_S$ Card No. {21-1272}. TiO_2 supported on large surface area of HZSM-5 to enhance the photocatalytic activity of pristine TiO_2. The intense peak of TiO_2 [101] increases as the loading of TiO_2 increases, as well as the peak intensity of all peaks of zeolite decreases. This decrease in peak intensity may be due to the dilution effect of zeolite which is suggesting that TiO_2 homogeneously dispersed on the surface of the HZSM-5 zeolite [24]. To

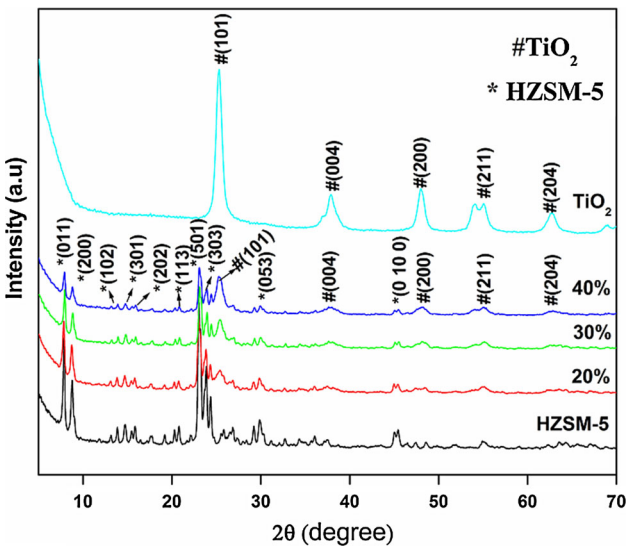

Fig. 1 XRD pattern of HZSM-5, TiO_2(20 %)/HZSM-5, TiO_2(30 %)/HZSM-5, TiO_2(40 %)/HZSM-5 and TiO_2

find out optimal amount of active material on HZSM-5 the amount of TiO_2 was varied from 20 to 40 wt%. The XRD patterns of different loading of TiO_2 on HZSM-5 are shown in Fig. 1. The average crystallite size of supported samples was calculated from the Scherrer's equation [25],

$$t = \frac{0.9\lambda}{\beta \cos\theta} \quad (1)$$

where t is the crystallite size, λ is the wavelength of X-ray, β is the full width at half maximum in radian and θ is the diffraction angle in degree. It is observed that, the average crystallite size of pristine TiO_2 is 15 nm whereas it decreases up to 12 nm for optimal photocatalyst [TiO_2(30 %)/HZSM-5].

Therefore an optimum temperature of 400 °C was chosen as a calcination temperature throughout the experiment. At 400 °C the 30 % TiO_2 on HZSM-5 found to be effective photocatalyst due to their crystallite size. The XRD patterns of TiO_2/HZSM-5 photocatalyst at different calcination temperature (300–600 °C) are shown in Fig. 2. Predominantly anatase phase is observed and no any additional peaks of rutile phase are found in the diffraction patterns of supported samples. This indicates that the anatase phase is found to be stable by the present experimental conditions. As the calcination temperature increases from 300 to 600 °C the XRD peaks gradually becomes sharp in nature indicating bigger size of crystals [24].

3.1.2 TEM of TiO_2/HZSM-5

The TEM image (Fig. 3a) of TiO_2 (30 %)/HZSM-5 photocatalyst gives more evidence and information about the morphology and special distribution of TiO_2 nanoparticles located at the surface of HZSM-5. The particle size of supported TiO_2 nanoparticles is 12 nm. High resolution TEM gives strong confirmation about the supported TiO_2 nanoparticles on the surface of zeolite. The image (Fig. 3b) of optimal photocatalyst indicates that, the interplanar distance (d) is about 0.35 nm, which is well accordance to [101] plane of anatase TiO_2. These results are in agreement with that of XRD.

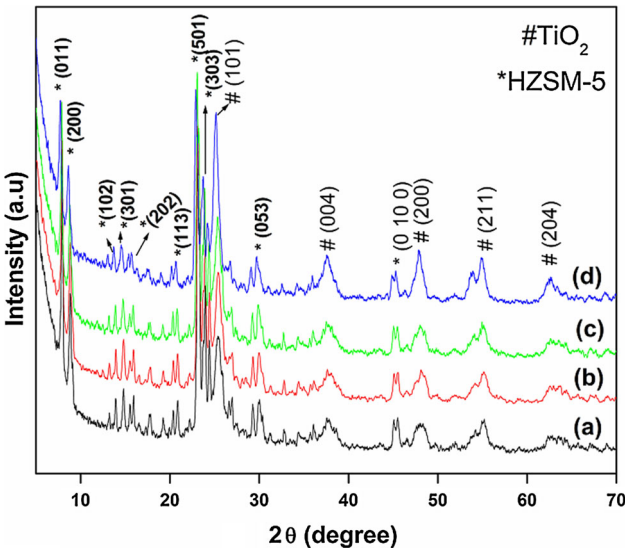

Fig. 2 XRD pattern of TiO_2(30 %)/HZSM-5 calcined at *a* 300 °C *b* 400 °C *c* 500 °C and *d* 600 °C

3.1.3 SEM and EDS of TiO_2/HZSM-5

The surface morphology of pristine and zeolite supported TiO_2 was studied by using SEM. Figure 4 shows the SEM images of pristine TiO_2 and TiO_2(30 %)/HZSM-5. As shown in Fig. 4a the morphology of TiO_2 is pseudo-cube like in nature. According to the SEM image of Fig. 4b the surface of zeolite is smooth, however it can be seen that the layer of TiO_2 nanoparticles exist on surface of HZSM-5. Also, mapping of elements are determined for TiO_2 (30 %)/HZSM-5 which is shown in Fig. 5a. In addition, the elemental analysis was performed by energy dispersive spectroscopy (EDS) and shown in Fig. 5b. It indicates the presence of Ti species on the surface of zeolite.

3.1.4 FT-IR of TiO_2/HZSM-5

Figure 6 shows the FT-IR spectra of pristine TiO_2, pure zeolite and TiO_2(20–40 %)/HZSM-5 in the range of 4000–400 cm^{-1}. The broad peak around 3416 and 1644 cm^{-1} are due to OH stretching and OH bending mode of vibration of adsorbed water of TiO_2 respectively. HZSM-5 is composed of tetrahedral skeleton of Si–O and Al–O bonds, so that the characteristic peak of Si–O is attributed to 556 cm^{-1}, and the peaks between 500 and 850 cm^{-1} can be assigned to vibration of Al–O in the framework of zeolite. [26]. The peak at 1105 cm^{-1} can be observed due to Si–O–Si bond. In contrast to their original pattern of FT-IR spectra (TiO_2 and zeolite), the spectra of TiO_2/HZSM-5 noticeably changed. The broad peak observed between 800 and 400 cm^{-1} owing to the superposition of Ti–O and Si–O bond. The characteristic peak of Si–O–Si shifts from 1049 to 1059 cm^{-1} which may be due to the interrelationship of TiO_2 and zeolite. The band at 960 cm^{-1} was not observed, which could be due to the antisymmetric stretching vibration of the Ti–O–Si bonds. Hence there will be no substitution of tetrahedral Si sites by Ti during the preparation of supported TiO_2 [27].

3.1.5 BET surface area of TiO_2/HZSM-5

The surface area is greatly influenced for the photocatalytic efficiency of TiO_2 and zeolite supported TiO_2 nanomaterials.

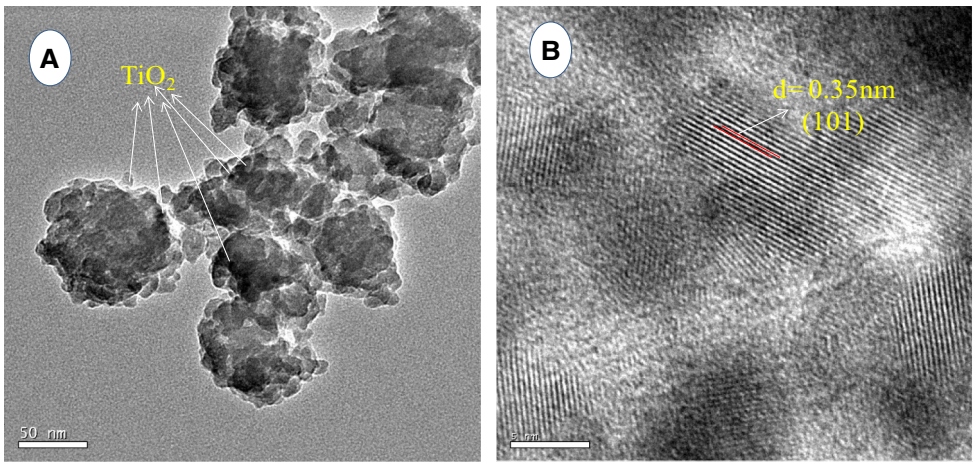

Fig. 3 **a** TEM image of TiO_2(30 %)/HZSM-5 and **b** HRTEM image of TiO_2(30 %)/HZSM-5

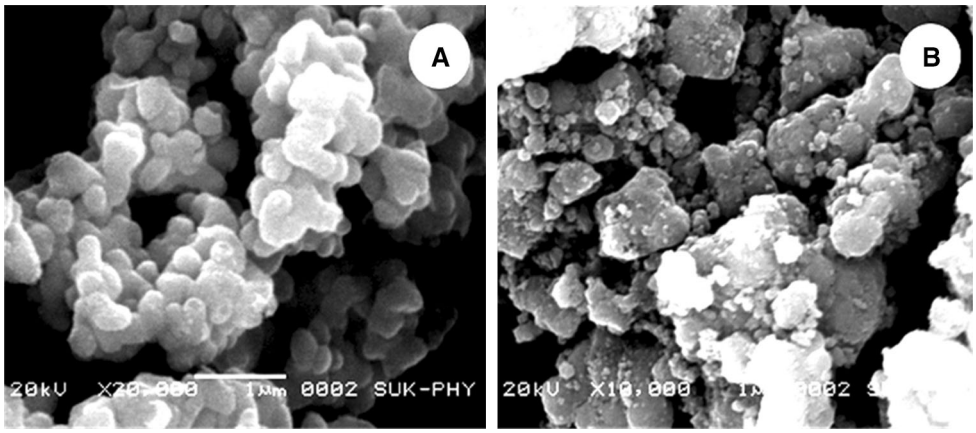

Fig. 4 SEM images of **a** Pristine TiO_2 and **b** TiO_2(30 %)/HZSM-5

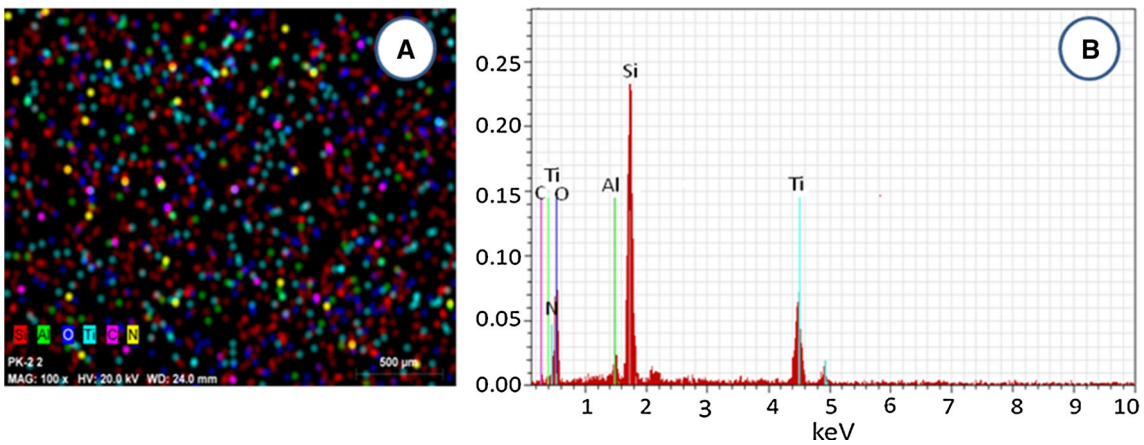

Fig. 5 EDS of TiO_2(30 %)/HZSM-5 **a** mapping and **b** elemental analysis

Due to the maximum surface area of photocatalyst, there may be an enhancement in the availability of adsorption sites and consequently avoids the recombination of the photogenerated electron–hole pair, thus there is an increase in the rate of photocatalysis [28]. As the wt% loading of TiO_2 increases the surface area decreases, as presented in Table 1. On the other hand, the S_{BET} of TiO_2 (30 %)/HZSM-5 calcined at different temperature decreases with increase in calcination temperature. For 400, 500 and 600 °C samples, the surface areas 307, 281 and 246 m^2/g respectively. Several authors [29] have reported that, the photocatalytic activity of nanomaterials is greatly affected by sintering temperature,

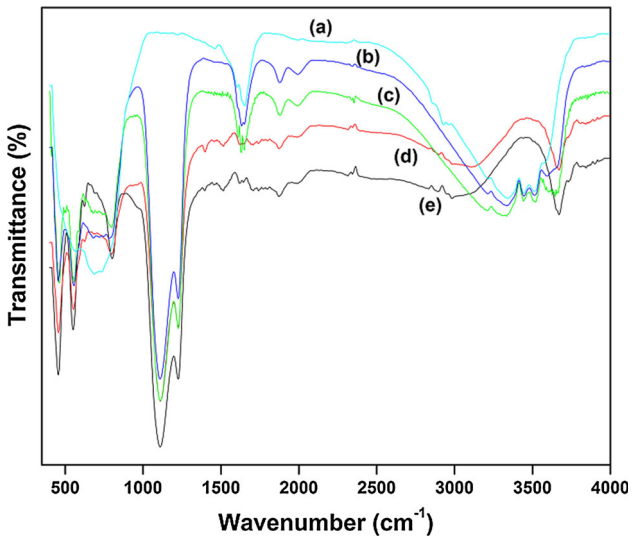

Fig. 6 FT-IR spectra of *a* TiO_2, *b* TiO_2(40 %)/HZSM-5 *c* TiO_2(30 %)/HZSM-5 *d* TiO_2(20 %)/HZSM-5 and *e* HZSM-5

Table 1 Surface area of different wt% loading of TiO_2 on HZSM-5

Sample	S_{BET} (m^2/g)
HZSM-5	344
TiO_2/HZSM-5 (20 %)	321
TiO_2/HZSM-5 (30 %)	307
TiO_2/HZSM-5 (40 %)	230
TiO_2	139

increasing the temperature up to 600 °C, surface area goes on decreases. This could be attributed to the agglomeration of TiO_2 and growth phenomenon during the calcination process. Our results suggest that TiO_2 supported on HZSM-5 has somewhat higher activity which is calcined at lower temperature.

3.1.6 DRS spectra of TiO_2/HZSM-5

The optical response of the prepared TiO_2/HZSM-5 nanomaterials was investigated by diffuse reflectance spectroscopic measurement. Figure 7 includes the spectra of pure HZSM-5, TiO_2/HZSM-5 calcined at 400 °C with different amounts of TiO_2 loading and pristine TiO_2. The initial HZSM-5 material exhibits a very low UV absorption whereas pristine TiO_2 shows absorption at 380 nm. However, titanium modified zeolite material shows different spectra than pure HZSM-5. The absorption ability of TiO_2/HZSM-5 catalyst is in between TiO_2 and HZSM-5, supported catalyst shows absorption edge at a shorter wavelength than that of pure TiO_2. A low content of TiO_2

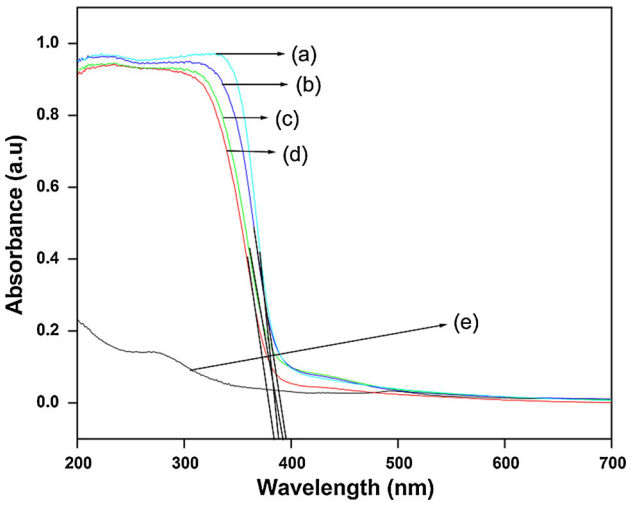

Fig. 7 DRS of *a* TiO_2 *b* TiO_2(40 %)/HZSM-5 *c* TiO_2(30 %)/HZSM-5 *d* TiO_2(20 %)/HZSM-5 and *e* HZSM-5

loading, the absorption edge is decreased. This suggest that, the particle size of TiO_2 supported HZSM-5 is smaller than that of pristine TiO_2.

3.2 Photocatalytic activity

3.2.1 Effect of TiO_2 loading on HZSM-5

In the present work TiO_2 has been synthesized on the surface of zeolite. Taking into consideration that the gel prepared by hydrolysis of TTIP has sufficient flexibility to penetrate into the zeolite structure and can distribute on the surface of holes and channels of zeolite structure due to the surface polarity could lead to strong interactions between the growing titania particles during the formation of sol–gel and the surface groups of the HZSM-5 [30]. The interaction between the surface of zeolite support and the TiO_2 precursor species could play a similar role than that occurring during template assisted syntheses of sol–gel TiO_2 in which the influence of incorporated functional groups has been pointed out during the hydrolysis step. [31]. Thus there will be exist strong bonding between oxygen atoms of TiO_2 nanoparticles and aluminosilicate framework of zeolite structure; so that washing the product for several times or stirring in an aqueous solution cannot separate TiO_2 from the zeolite. Thus it can be concluded that these interactions between TiO_2 and the framework of zeolite are significantly strong and could not be break easily [32].

Therefore the effect of TiO_2 loading on the HZSM-5 for the degradation of AG 25 was studied which is shown in Fig. 8. The optimal 0.1 g/dm^3 photocatalyst was used in 100 mL of AG 25 solution. The percentage degradation of

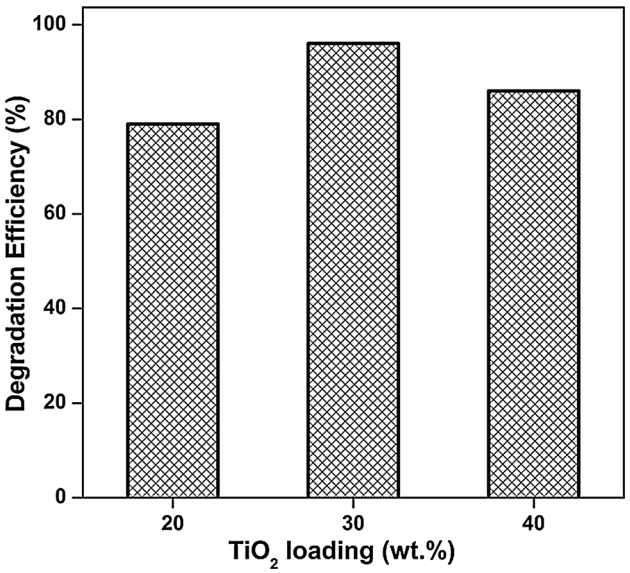

Fig. 8 Effect of TiO_2 loading on HZSM-5

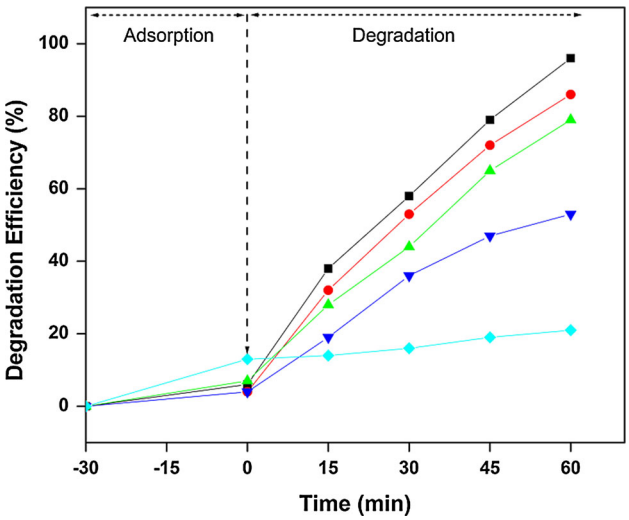

Fig. 9 Effect of photocatalyst and loading of TiO_2 on the degradation of Acid Green-25

samples was calculated by using the following equation [30],

$$X = \frac{Co - Ct}{Co} \times 100 \quad (2)$$

where C_0 is the original concentration and C_t is the remaining concentration of AG 25 solution after certain time interval. As it can be seen from the figure that, the percentage degradation was increased up to 30 wt% and then decreases on further loading of TiO_2. Considering XRD results shown in Fig. 1, the lower photocatalytic activity of TiO_2 (20 %)/HZSM-5 may result from crystalline nature of TiO_2 while the low activity of TiO_2 (40 %)/HZSM-5 could be due to decrease in surface area by the agglomeration of TiO_2. The surface area of TiO_2 (40 %)/HZSM-5 is shown in Table 1. Figure 9 shows the comparative study for photodegradation of AG 25 with pristine TiO_2, HZSM-5 and supported photocatalyst. The TiO_2 shows 53 % whereas HZSM-5 has no significant degradation (7 %). This observation confirms that, HZSM-5 is not photoactive by itself for degradation of AG 25. Figure 10 indicates the UV–Vis absorption spectra of optimized TiO_2 (30 %)/HZSM-5 supported photocatalyst which shows highest photodegradation of AG 25 under UV-light irradiation.

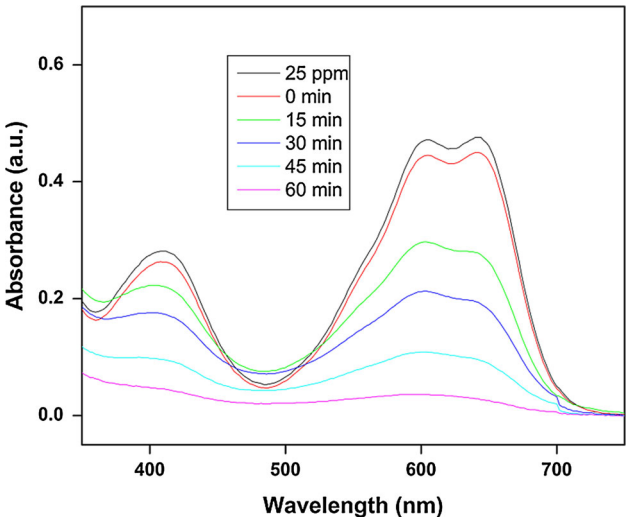

Fig. 10 UV–visible absorption spectra of Acid Green-25 degradation under UV-light using TiO_2(30 %)/HZSM-5

3.2.2 Effect of calcination temperature

Several parallel samples of the zeolite supported by titania, calcined at different temperatures in the range of 300–600 °C were studied. Figure 11 shows the catalytic activity of TiO_2(30 %)/HZSM-5 as a function of calcination temperature. The photocatalytic activity of supported TiO_2 decreased from 96 to 87 % of the samples calcined between the temperature ranges from 400 to 600 °C. This could be due to large particle size with temperature. This is well attributed to the surface area and XRD results, as higher temperature produces larger crystallites and lower surface area over the zeolite surface [33].

3.2.3 Effect of catalyst content

The reaction rate as a function of catalyst content is an important factor quantitatively. Hence a series of experiments were carried out to find the optimal content of TiO_2/HZSM-5 for degradation of AG 25. The amount of photocatalyst was varied from 0.05 to 0.125 g/dm^3 keeping all

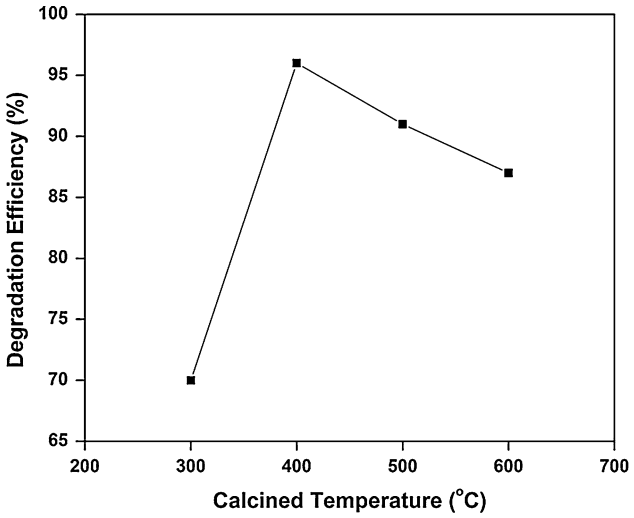

Fig. 11 Effect of calcination temperature on photodegradation of Acid Green-25

other experimental parameters identical and shown in Fig. 12. The rate of photodegradation was increased with an increase in catalyst amount from 0.05 to 0.1 g/dm^3. However, further increment in the catalyst amount leads to reduction in degradation efficiency. Akpan et al. [34] reported that, the amount of catalyst has both positive and negative impacts on the photodegradation phenomenon. If the concentration of the catalyst is beyond 0.1 g/dm^3, the adsorption on catalyst surface and absorption of light by catalyst are the limiting factors. However, at higher catalyst amount, there is an increase in turbidity of the solution. As a result a decrease in photo-active sites leads to decrease in degradation efficiency of AG 25 solution.

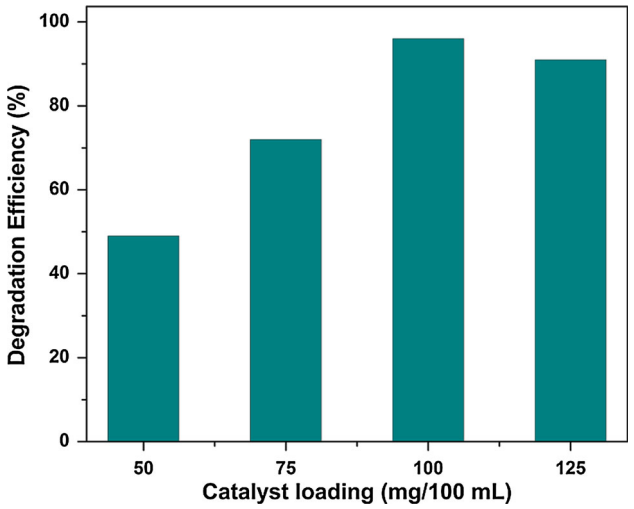

Fig. 12 Effect of TiO_2(30 %)/HZSM-5 catalyst loading for degradation of Acid Green-25

4 Conclusions

A photocatalyst containing TiO_2 was modified by using HZSM-5 as a support and synthesized with an energy efficient microwave assisted method. The obtained material did not show the evidence of rutile phase, whereas anatase phase was solely observed. The results of present investigation suggest that the best photocatalyst is TiO_2(30 %)/HZSM-5. An average crystallite size of 12 nm was obtained which is less than pristine TiO_2 (15 nm). An improvement in surface area of catalyst plays an important role to enhance photocatalytic activity. The band gap was slightly changed with TiO_2 content. Hence, by the studying of all these variables it can be concluded that, the catalytic activity of optimal photocatalyst [TiO_2(30 %)/HZSM-5] shows highest photodegradation. It shows a maximum 96 % photodegradation of AG 25 (25 ppm) within 60 min under UV light irradiation at 0.1 g/dm^3 loading of photocatalyst.

Acknowledgments One of the authors (KMG) thankful to DST, New Delhi for financial support under Major Research Project (SR/S1/PC/0041/2010).

References

1. S.Y. Ryu, J. Choi, W. Balcerski, T.K. Lee, M.R. Hoffmann, Ind. Eng. Chem. Res. **46**, 7476–7488 (2007)
2. P. Raja, J. Bandara, P. Giordano, J. Kiwi, Ind. Eng. Chem. Res. **44**, 8959–8967 (2005)
3. X. Hu, G. Li, J.C. Yu, Langmuir **26**, 3031–3039 (2010)
4. A.S. Weber, A.M. Grady, R.T. Koodali, Catal. Sci. Technol. **2**, 683–693 (2012)
5. R. Daghrir, P. Drogui, D. Robert, Ind. Eng. Chem. Res. **52**, 3581–3599 (2013)
6. H. Park, Y. Park, W. Kim, W. Choi, J. Photochem. Photobiol. C **15**, 1–20 (2013)
7. B. Cheng, Y. Le, J. Yu, J. Hazard. Mater. **177**, 971–977 (2010)
8. Y. JiL, C. Wei, Catal. Sci. Technol. **1**, 802–809 (2011)
9. S. Izadyar, S. Fatemi, Ind. Eng. Chem. Res. **52**, 10961–10968 (2013)
10. Y. Kuwahara, H. Yamashita, J. Mater. Chem. **21**, 2407–2416 (2011)
11. S. Yamaguchi, T. Fukura, Y. Imai, H. Yamaura, H. Yahiro, Electrochim. Acta **55**, 7745–7750 (2010)
12. M.B. Suwarnkar, R.S. Dhabbe, A.N. Kadam, K.M. Garadkar, Ceram. Int. **40**, 5489–5496 (2014)
13. I. Paramasivam, A. Avhale, A. Inayat, A. Bosmann, P. Schmuki, W. Schwieger, Nanotechnology **20**(225607), 5 (2009)
14. M.E. Roz, L. Lakiss, J.E. Fallah, O.I. Lebedev, F.T. Starzyk, V. Valtchev, Phys. Chem. Chem. Phys. **15**, 16198–16207 (2013)
15. C.S. Triantafillidis, A.G. Vlessidis, L. Nalbandian, N.P. Evmiridis, Microporous Mesoporous Mater. **47**, 369–388 (2001)
16. F. Bin, C. Song, G. Lv, J. Song, X. Cao, H. Pang, K. Wang, J. Phys. Chem. C **116**, 26262–26274 (2012)
17. A.S. Al-Dughaither, H.D. Lasa, Ind. Eng. Chem. Res. **53**, 15303–15316 (2014)
18. J.K. Reddy, V. Durgakumari, M. Subrahmanyam, B. Sreedhar, Mater. Res. Bull. **44**, 1540–1546 (2009)

19. D.A. Young, A.K. Mohammed, S.K. Blue, K.L. Roberts, J. Chem. Proc. Eng. **1**, 203 (2014)
20. R. Koswojo, R.P. Utomo, Y.H. Ju, A. Ayucitra, F.E. Soetaredjo, J. Sunarso, S. Ismadji, Appl. Clay Sci. **48**, 81–86 (2010)
21. V.P. Shiralkar, P.N. Joshi, M.J. Eapen, B.S. Rao, Zeolites **11**, 511–516 (1991)
22. H. van Koningsveld, H. van Bekkum, J.C. Jansen, Acta Cryst. B **43**, 127–132 (1987)
23. G.V. Khade, M.B. Suwarnkar, N.L. Gavade, K.M. Garadkar, J. Mater. Sci. Mater. Electron. **26**, 3309–3315 (2015)
24. S. Gomez, C.L. Marchena, L. Pizzio, L. Pierella, J. Hazard. Mater. **258**, 19–26 (2013)
25. M.S. Lee, S.S. Hongb, M. Mohseni, J. Mol. Catal. A Chem. **242**, 135–140 (2005)
26. C. Wang, H. Shi, Y. Li, Appl. Surf. Sci. **257**, 6873–6877 (2011)
27. W. Zhang, F. Bi, Y. Yu, H. He, J. Mol. Catal. A Chem. **372**, 6–12 (2013)
28. R.M. Mohamed, A.A. Ismail, I. Othman, I.A. Ibrahim, J. Mol. Catal. A Chem. **238**, 151–157 (2005)
29. Y. Xu, C.H. Langford, J. Phys. Chem. B **101**, 3115–3121 (1997)
30. M. Khatamian, S. Hashemian, A. Yavari, M. Saket, Mat. Sci. Eng. B **177**, 1623–1627 (2012)
31. T. Klimnova, E. Carmona, J. Ramirez, J. Mater. Sci. **33**, 1981 (1998)
32. M. Lafjaha, F. Djafri, A. Bengueddach, N. Keller, V. Keller, J. Hazard. Mater. **186**, 1218–1225 (2011)
33. M. Khan, W. Cao, J. Mol. Catal. A Chem. **376**, 71–77 (2013)
34. U.G. Akpan, B.H. Hameed, J. Hazard. Mater. **170**, 520–529 (2009)